Radio Science

RESEARCH ARTICLE
10.1029/2024RS008140

# Monitoring Global Ionospheric Conditions With Electromagnetic Lightning Impulses Registered in Extremely Low Frequency Measurements

**Z. Nieckarz[1], M. Gołkowski[2], J. Kubisz[3], M. Ostrowski[3], A. Michalec[3], J. Mlynarczyk[4], J. Lichtenberger[5,6], and A. Maxworth[7]**

[1]Marian Smoluchowski Institute of Physics, Jagiellonian University, Kraków, Poland, [2]Department of Electrical Engineering, University of Colorado Denver, Denver, CO, USA, [3]Astronomical Observatory, Jagiellonian University, Kraków, Poland, [4]Institute of Electronics, AGH University of Science and Technology, Kraków, Poland, [5]Department of Geophysics and Space Sciences, Eötvös University, Budapest, Hungary, [6]HUN-REN-ELTE Space Research Group, Budapest, Hungary, [7]Department of Engineering, Gorham, ME, USA

**Key Points:**

- Strong thunderstorm lightning generated EM impulses may serve as a measuring tool for ionospheric conditions at global scale distances
- Diurnal changes in ELF impulse speeds differ between meridional and latitudinal paths
- The X-ray solar flares (here M8-class) modulate ELF impulse propagation depending on flux and signal path orientation on Earth

**Correspondence to:**
Z. Nieckarz,
zenon.nieckarz@uj.edu.pl

**Citation:**
Nieckarz, Z., Gołkowski, M., Kubisz, J., Ostrowski, M., Michalec, A., Mlynarczyk, J., et al. (2025). Monitoring global ionospheric conditions with electromagnetic lightning impulses registered in extremely low frequency measurements. *Radio Science*, *60*, e2024RS008140. https://doi.org/10.1029/2024RS008140

Received 7 OCT 2024
Accepted 14 FEB 2025

**Author Contributions:**
**Conceptualization:** Z. Nieckarz, M. Gołkowski, M. Ostrowski
**Data curation:** Z. Nieckarz, M. Gołkowski, J. Kubisz, A. Michalec, J. Mlynarczyk, J. Lichtenberger, A. Maxworth
**Formal analysis:** Z. Nieckarz, M. Gołkowski
**Investigation:** Z. Nieckarz, J. Kubisz, M. Ostrowski, A. Michalec, J. Mlynarczyk, A. Maxworth
**Methodology:** Z. Nieckarz, M. Gołkowski, J. Kubisz, M. Ostrowski
**Resources:** Z. Nieckarz, M. Gołkowski, A. Michalec, J. Mlynarczyk, J. Lichtenberger
**Validation:** Z. Nieckarz, M. Gołkowski, J. Kubisz, M. Ostrowski, A. Michalec, J. Mlynarczyk, J. Lichtenberger, A. Maxworth
**Visualization:** Z. Nieckarz
**Writing – original draft:** Z. Nieckarz, M. Gołkowski, M. Ostrowski, J. Lichtenberger
**Writing – review & editing:** Z. Nieckarz, M. Gołkowski, M. Ostrowski



**Abstract** The Extremely Low Frequency band (ELF: 0.03–1,000 Hz) electromagnetic signals from thunderstorm lightning discharges can propagate around the globe in the Earth-ionosphere resonance cavity and thus be used for ionosphere monitoring. We use ELF observations of impulses detected by the World Wide Lightning Location Network (WWLLN) to investigate ELF propagation velocity and arrival azimuth under diurnal changes over 2 days in September 2023. Also, temporary effects of solar flares' ionizing fluxes are monitored, leading to increase of the ELF signal propagation speed in proportion to the X-ray flux intensity. We present a simple method for automatic and large-scale analysis, utilizing data from two registration systems (our ELF reciever and WWLLN) and enabling easy evaluation of changes in wave propagation speed. Comparative analysis of WWLLN identified impulses generated in Africa and America reveals varying effects of signal refraction, with increased azimuth changes for signals propagating across the ionospheric ionization gradients associated with the day/night terminator. The method has a potential to become a standard tool for the analysis and monitoring of the lower layers of the ionosphere.

**Plain Language Summary** This text explains how extremely low frequency (ELF) electromagnetic waves, generated by lightning discharges, can propagate around the Earth. These signals are used to monitor the state of the ionosphere. The study focuses on signals from 2 days in September 2023, showing how ELF signal propagation speed and arrival direction change due to daily variations and the impact of X-ray radiation from solar flares. Specifically, the study analyzes signals from lightning discharges occurring over Africa and America, observing different refraction effects caused by ionization changes in the ionosphere.

## 1. Introduction

Natural electromagnetic waves measured on Earth at extremely low frequencies (ELF) are primarily generated by atmospheric lightning discharges. Due to their long propagation paths within the spherical Earth-ionosphere cavity, globally generated ELF waves can be investigated using a detector in a single location (see, for example, Nickolaenko & Hayakawa (2002), or the recent review by Liu et al., 2023). As ELF wave propagation depends on parameters of the ionosphere, in particular on varying ionization degrees of the lower ionospheric layers and their nonuniformities, one can study ionospheric structures with knowledge of the emission source position with respect to the signal receiver. Global lightning locations are available from the WWLLN network (Rodger et al., 2004; https://wwlln.net) or Vaisala network (Said & Murphy, 2016; https://www.vaisala.com). Identification of lightning signatures in ELF data enables continuous monitoring of the lower ionosphere on a global scale which is a longstanding challenge (Anderson et al., 2020; Burkholder et al., 2013; Gołkowski et al., 2021). ELF waves have unique properties that make them particularly sensitive to the electron density gradients of the lower ionosphere (Golkowski et al., 2018).

The majority of past efforts on remote sensing of the lower ionosphere have been done in the VLF (3–30 kHz) band (see review by Barr et al., 2000). The VLF band offers the advantage of controlled anthropogenic sources in the form of military communication transmitters, which allow for the observation of perturbations of VLF amplitude and phase. However, VLF propagation in the Earth-ionosphere is multi-modal, meaning that its

perturbation leads to a nonlinear response. This has made unambiguous determination of ionosperic perturbations from VLF observations challenging, especially with a small number of receivers (Gołkowski et al., 2021). Recent efforts to improve VLF remote sensing have extended to machine learning (Gross & Cohen, 2020), polarization (Burch & Moore, 2024), or jointly analyzing VLF transmitter and lightning signatures (Richardson & Cohen, 2023).

The ELF band does not have easily exploitable controlled sources and the noise environment is more challenging than for VLF. The dominant source of noise in ELF measurements are non-propagating near-fields from electrical power infrastructure. However, ELF propagation involves only one propagating mode and due to significant dispersion, the propagation and phase velocities are a function of the ELF frequency and the ionospheric electron density. The fields associated with ELF waves also penetrate the ionsphere to a higher altitude than VLF fields, making them a useful probe over a larger portion of the lower ionosphere. A comparison of ELF and VLF propagation chracteristics is provided by Bannister (1984). Before accurate lightning detection was available on global scale, the majority of ionspheric sensing with ELF waves focused on Schumann resonances (Nickolaenko & Hayakawa, 2002). The present work follows on from the study of Gołkowski et al. (2018), which first considered the use of observed ELF group velocity from lightning impulses of know location and occurrence time as a diagnostic tool of the lower ionosphere along the propagation path.

We present an automatic method for identifying impulses associated with WWLNN lightning events in magnetic ELF data from our geophysical Hylaty station in Poland. For these identifications we use impulse arrival time and derive propagation speed and azimuth and eventual deviation from the geographic azimuth.

Below, we present analysis results for 2 days, 20 and 21 September, 2023. The approach presented here focuses on individual lightning events with known source information. Due to improved timing accuracy and identification algorithms, the present work yields higher fidelity group velocity signatures of ionospheric changes than earlier work presented by Gołkowski et al. (2018).

## 2. Analyzed Data and Methods

### 2.1. Data Sources

In this study, ELF data recorded by our ELA11 sensor from two magnetic antennas (NS, EW), were utilized. The sensor ELA11 is installed at the geophysical station Hylaty (Kulak et al., 2014; Nieckarz, 2016) in the southeast of Poland (49.2°N, 22.5°E), and operates with sampling frequency of 3 kHz with an operational bandwidth of 0.03–1,000 Hz. It employs an 18-bit analog to digital converter and orthogonal EW and NS magnetic antennas (1 sensor unit [s.u.] corresponds to a magnetic field change of 78.86 fT, or 1 pT = 12.68 s.u.) to continuously monitor natural electromagnetic waves in the ELF band. The use of an analog Bessel anti-aliasing filter enables very good resolution of individual impulses in the recorded signal.

A reference data set on atmospheric discharges utilized in the study is provided by the WWLLN system (Rodger et al., 2004; https://wwlln.net), which operates in the very low frequency (VLF, 3–30 kHz) band. This system provides global data on major lightning discharges on Earth, including a time of each large discharge and its location. As presented in Figure 1a, in the present study we compare results from the sets of WWLLN discharges selected from wide range of azimuths from Africa and Central America, with distances between 5 and 9 Mm. On the figure one can note quite different ranges of ELF impulse trajectories with respect to the solar irradiation conditions, and thus the ionosphere structure.

The study also utilizes measurement results from the extreme ultraviolet sensor (EUVS) and the X-ray sensor measurements (XRSA) recorded by the GOES-16 satellite. The data binned in 1-min intervals were obtained for the days of 20 and 21 September, 2023, from https://www.ngdc.noaa.gov/stp/satellite/goes-r.html.

### 2.2. Method of Pulse Identification

Following earlier application by Nieckarz et al. (2011) a procedure of identifying ELF impulses originating from discharges detected by the WWLLN system is illustrated in Figure 1. To minimize signal perturbations caused by the 50 Hz electric power lines emission, we use a software third-order bandstop Butterworth filter to remove these fluctuations, as described in detail in Kubisz et al. (2024). In the first step, the ELF signals from both antennas were subjected to an identical transformation, which consists of subtracting from each data sample the average

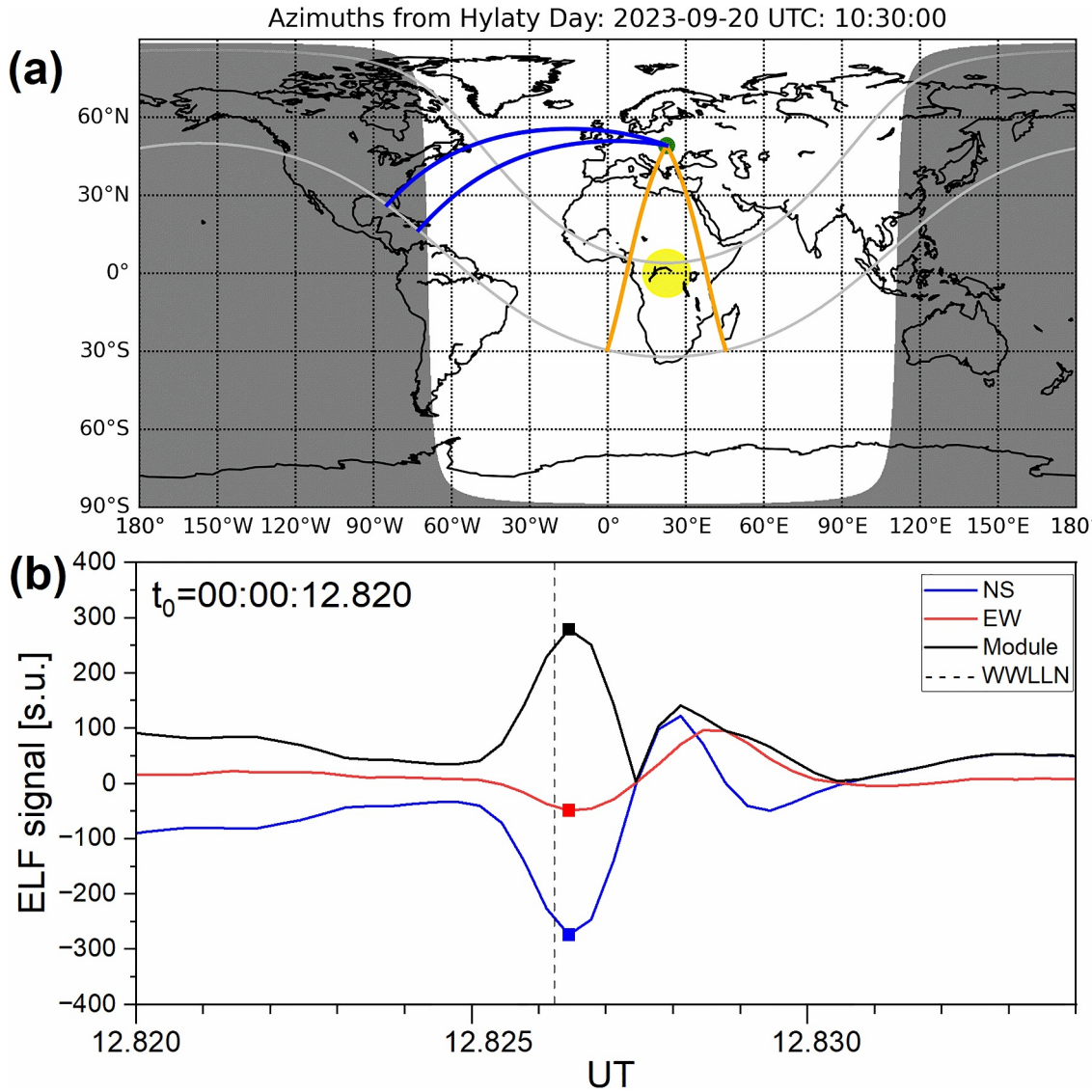


**Figure 1.** (a) Illustration of the solar irradiation pattern on Earth on 20 September, 2023, 10:30 UT. and the ranges azimuths (sectors between orange and blue lines) and distances (between gray lines) for the studied WWLLN events. The Sun position is indicated by a large yellow spot, a position of the Hylaty station by a green dot. (b) ELF electromagnetic measurements from both antennas (NS, EW) and a module $M$ of the ELF signal for a 14 ms period starting on 20 September, 2023, at 00:00:12.820 UT. The black square marks a position of the detected $M > 200$ s.u. peak in the ELF signal module waveform. The vertical dashed line indicate the predicted reference time $t_p$ for expected detection of the WWLLN event. On the figure the fitted impulse parameters are $B_{NS} = -274.18$ s.u.; $B_{EW} = -49.07$ s.u.; $A_{\mathrm{ELF}} = 100.1°$; $Ag = 100.5°$; $\Delta t = 0.218$ ms.

value calculated from the 67 ms (200 samples) time range preceding the signal sample in question. Then, from the waveforms thus transformed, the ELF signal modulus $M$ waveform was calculated according to formula $M = \mathrm{SQRT}(B_{\mathrm{EW}}{}^2 + B_{\mathrm{NS}}{}^2)$. An example of these three ELF waveforms is shown in Figure 1.

From the WWLLN system, we know the moment when the atmospheric discharge occurred ($t_{\mathrm{WWLLN}}$) and its location on the globe. The WWLN location accuracy is on the order of a few kilometers and its timing accuracy is on the order of a few microseconds. Consequently, we derive the distance ($D$) along the Earth surface between the discharge location and the ELF receiver. Then, an "reference" time of the impulse arrival to the ELF sensor, $t_p = \mathrm{D}/v + \Delta t_{\mathrm{sens}}$, is calculated for the assumed wave propagation speed of $v = 0.85c$ (where: $c$ is the speed of light in vacuum; the factor of 0.85 was adopted from the work by Gołkowski et al. (2018), where it roughly represents the midpoint of the v/c range) and the ELF sensor signal delay $\Delta t_{\mathrm{sens}}$ is measured to be 1.87 ms. On Figure 1 such reference time is marked with a vertical dashed line. Subsequently, in the ELF signal magnitude waveform,

we identified peaks with amplitudes $M$ of at least 200 s.u., an arbitrarily chosen limiting value to select strong impulses allowing precise measurements. Then, the WWLLN event related peak is automatically identified by selecting the $M > 200$ impulse maximum nearest to the time $t_p$, with a measured time difference $\Delta t$.

The corresponding signals at times $t_{ELF} = t_p + \Delta t$ in the individual antennas $B_{NS}$ and $B_{EW}$ (see red and blue dots in Figure 1) were then used to calculate the impulse azimuth according to the formula $A_{ELF} = \arctan(-B_{NS}/B_{EW})$, where angles are derived in the range (−180°, 180°). With such arrangement the North direction is at $A = 0°$, the azimuth grows to the East and the South direction coincides with both limiting azimuths −180° and 180°. In parallel, based on the known geographic coordinates of the Hylaty station and the location of the atmospheric discharge, the geographic azimuth $A_g$ is calculated and the azimuth difference $\Delta A = A_{ELF} - A_g$ is computed for each studied discharge. Let us note that the impulses from our investigated African thunderstorm center presented at Figure 1a are characterized with azimuths up to 20° from the South, while the events from American direction are limited to the range $-60° < A_g < -75°$.

As illustrated in Figure 1b, the identified maximum in the ELF waveform at the time $t_{ELF}$ is delayed or ahead of the reference time $t_p$ by the time $\Delta t$ relative to the approximate signal arrival time, $t_{ELF} = t_p + \Delta t$. Knowing the distance $D$ and the measured propagation time of the ELF wave ($T_D = t_{ELF} - t_{WWLLN}$) the effective propagation velocity $v = D/T_D$ is calculated.

In the presented analysis, only those ELF identifications were used where the absolute value of $\Delta t$ is less than 6.5 ms and a difference between $A_g$ and $A_{ELF}$ is smaller than 30°, The applied time limit has been selected to reduce spurious results, but allow for different ELF wave velocities during the day and night, as well as refracted curved paths of ELF impulses. If more than one ELF signal maximum is found within the considered interval $|\Delta t| < 6.5$ ms, the case with the smallest azimuth angle difference is selected.

## 3. Results

Using the method described above for calculating the parameters $\Delta t$, $v$, and $\Delta A$, an analysis was performed for the 2 days of 20 and 21 September, 2023, during which the WWLLN system recorded 818,152 and 819,834 lightning discharges, respectively. For each day, an analysis was limited to two groups of discharges with propagation paths significantly different with respect to the ionosphere structure and terminator orientation, as illustrated on Figure 1a.

The first group consists of discharges for which the geographical azimuth $A_g$ is toward the South, between −160° and 160°, and the distance $D$ is between 5,000 and 9,000 km, limiting source locations to African thunderstorms. Let us note that during a passage of the terminator over the Hylaty station these impulses propagate at small angles to the day/night terminator line, oriented close to a local meridian in the considered dates. The second group of discharges are those for which $A_g$ is between −75° and −60° and the same distance range as above. The selected range of azimuths and distances thus limits the lightning sources to the so-called American center of thunderstorm activity. The Hylaty station has similar local time and longitude to the African lightning center while the local time of the American center is at 5–9 hr earlier. When inspecting evaluations of average parameters $\Delta t$, $v/c$ and $A$ for the figures below, one should note a significant scatter related to each such evaluation, which–in our opinion–can result from misidentified impulses, superposition of some background signal at the measurement, a non-delta-like original WWLLN impulses or wave trajectory perturbations by ionospheric non-uniformities. It requires a more detailed analysis not intended for the present paper.

In Figure 2, the results obtained for the African thunderstorm center on 20 and 21 September, 2023, are presented. The daily distribution of the time $\Delta t$ shows negative deviations (∼−2 ms) from a reference time $t_p$ during nighttime hours and smaller, negative deviations (∼−0.5 ms) during daytime hours. The transition from low to high values occurs in the morning between approximately 4 and 5 UT, while the transition from high to low values occurs in the evening between 16 and 17 UT. Thus a daily distribution of the parameter $v$/c shows higher values close to 0.95 during nighttime and lower values near 0.86 for the daytime signal propagation. It should be noted that the daily distribution of derived $v$/c parameters is a much like a mirror image of the $\Delta t$ curve, but with variations in times due to varying source distances not influencing the derived velocities. One should also note that velocities measured after the solar flare "spike" are significantly lower as compared to the ones before the flare. This effect we will discuss below Figure 4.

10.1029/2024RS008140

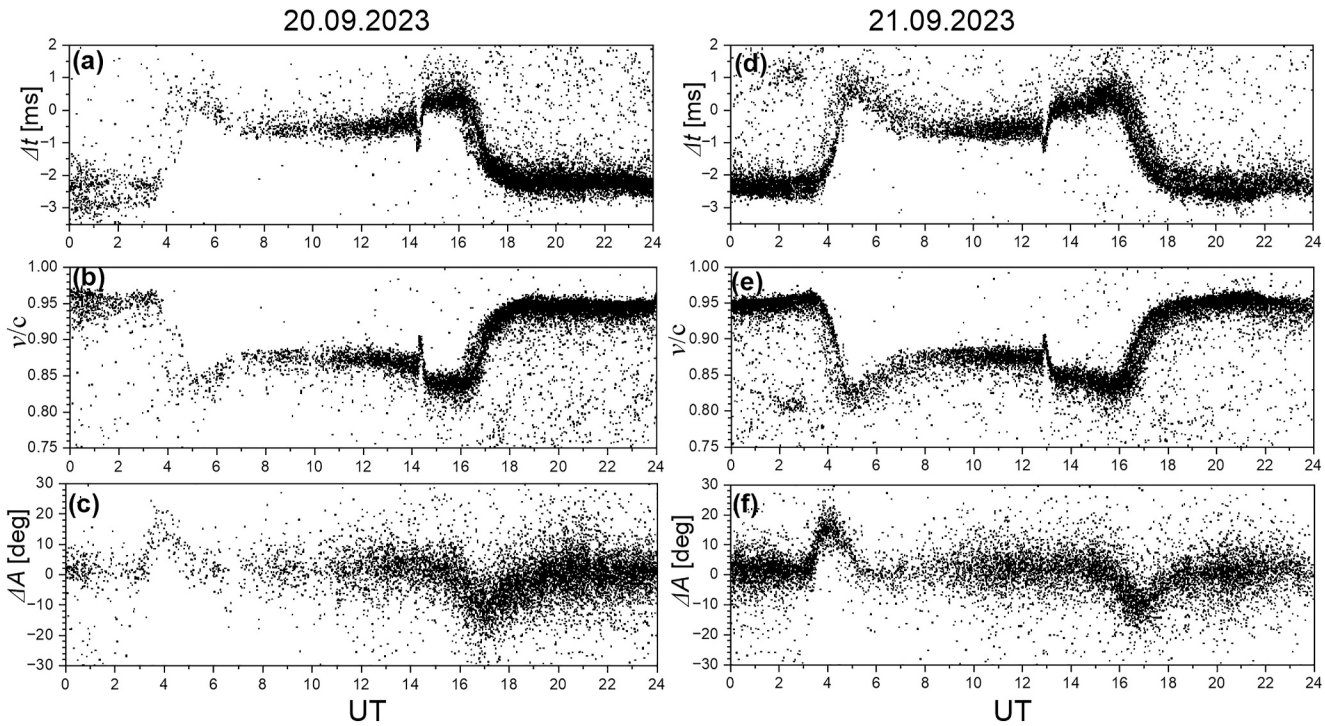


**Figure 2.** Daily distributions of parameters $\Delta t$ (panels a, d), $v/c$ (b, e) and $\Delta A$ (c, f) calculated for WWLLN lightning events in the above defined African thunderstorm center on 20th (left side) and 21st (right side) September , 2023. Sunrise and Sunset effects can be seen near 4:00 UT and 16:00 UT. A characteristic sharp dip (for $\Delta t$) or peak (for $v/c$) is visible in both days strictly coinciding with solar flares at 14:15 UT on 20 September and 12:50 UT on 21 September (see Figure 4). Two wavy azimuth change structures coincide with the terminator passage over the Hylaty station.

For these 2 days the daily distribution of the parameter $\Delta$A is horizontally flat with a mean value near +1.5°, but with a relatively large dispersion. It should be noted that around 4 UT the $\Delta$A distribution shows a wavy structure associated with the terminator transition, which reaches a value of about +15°, and around 17 UT a negative value of about −15°.

In Figure 3, the results obtained in the same 2 days for the American thunderstorm center are presented, showing significant differences as compared to the results for the African center in Figure 2. The daily distribution of the delay time $\Delta t$ shows small negative values (−2–−3 ms) during local nighttime hours at the receiver, from 0 to 4 UT, when the signal propagation proceeds in the night conditions and positive values (∼1 ms) during local daytime hours, from 12 to 16 UT, for propagation full within a day hemisphere. The relatively slow transition from night to day values occurs in the morning between 4 UT and 12 UT, when the terminator splits the signal trajectories for day and night parts. The later transition to the night values occurs in the evening between 17 UT and 24 UT, again with signal trajectories splitting in a growing proportion between day/night conditions. The daily distribution of the parameter $v$/c shows higher values (0.94) during nighttime and lower values (0.84) during daytime. A wavy feature in $v/c$ between 10 UT and 12 UT, with a maximum in between, is possibly generated by the passage of the day/night terminator over the lightning source region (see Figure 1a).

In contrast, the variation of the parameter $\Delta A$ from 0 to 6 UT is flat and averages about −9°, and from 5 to 13 UT the average value is about −2°, and with spread of values greater than in the previous hours. The following evolution of the $\Delta A$ values from 13 to 18 UT exhibits a significantly higher scatter of points in both days with respect to more compact earlier structure, in particular during the night. Only after 18 UT do the $\Delta A$ values again cluster around the −5° value and slowly decrease, reaching an average value of −9° from about 20 UT to 24 UT. We interpret these systematic changes as effects of refraction (Ostrowski et al., 2024) during propagation perpendicular to the ionosphere gradient at medium geographic altitudes (see Figure 1a), with possible influence of low ionosphere non-uniformities. It should be noted that the daily distributions of the analyzed parameters ($\Delta t$, $v/c$) obtained for both days are similar in general character for both groups of lightning discharges corresponding to African and American thunderstorm centers. On the other hand, clear differences are observed in

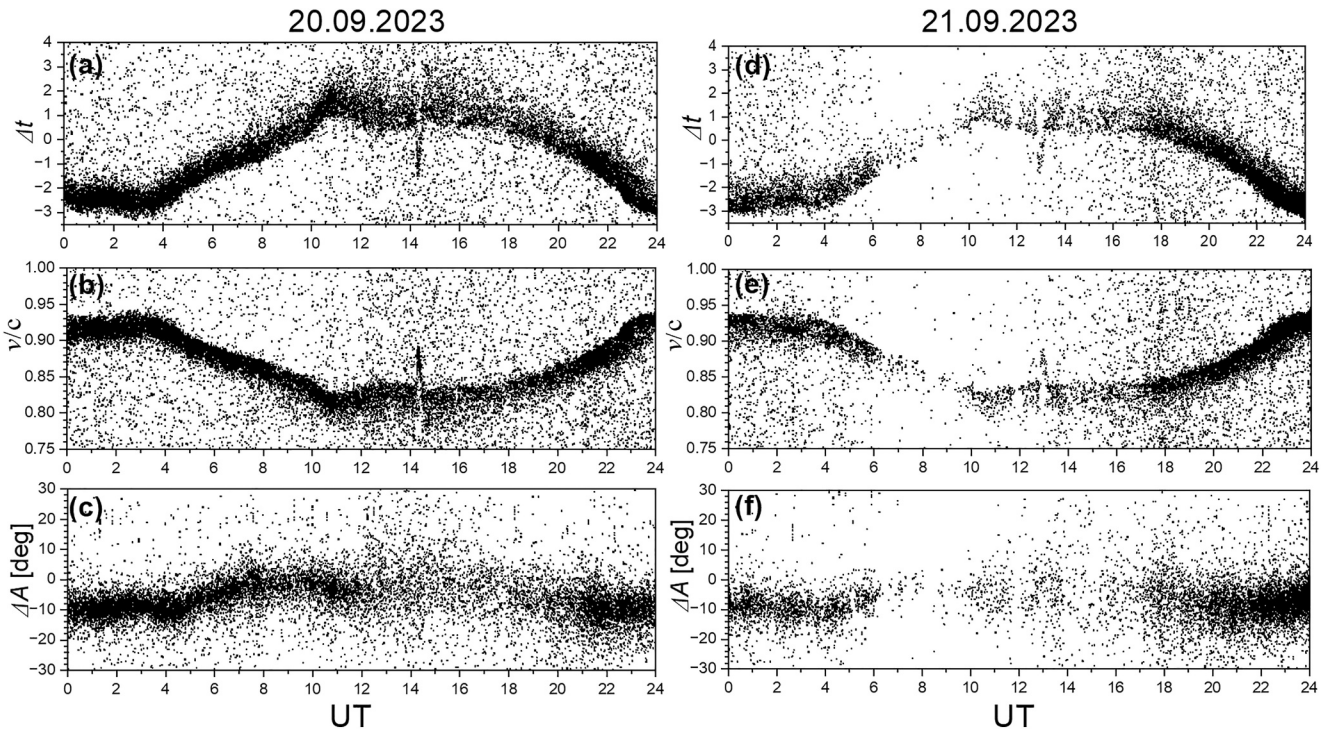


**Figure 3.** Daily distribution of parameters Δ*t* (panels a, d), *v*/*c* (b, e) and Δ*A* (c, f) calculated for WWLLN lightning events in the above defined American thunderstorm center on 20th (left side) and 21st (right side) September, 2023. In the plot noticeable differences are visible as compared to Figure 2, but the presence of solar flare generated sharp structures is clearly visible also here.

measured azimuth deviations Δ*A* due to different refraction effects of the measured impulse paths with respect to the terminator and the altitudinal ionospheric gradients.

Short-term solar flare generated variations in Δ*t* and *v*/*c* are observed after 14:15 on 20 September, 2023, and after 12:50 on 21 September, 2023. These variations are noticeable for both the African and American centers. Figure 4 presents the *v*/c variation profiles for both these centers alongside UV (140.4 nm) and XRSA (0.05–0.4 nm) radiation fluxes, as recorded by the GOES-16 satellite. It is evident that the observed changes in the *v*/*c* parameter correspond more closely with the X-ray XRSA radiation profile (with a 1–2 min delay) than with the shorter UV radiation profile. One should note for the African data (panels a, e; see also Figures 2b and 2f), that the signal velocities are lower after the flare, as compared to conditions before the flare. It is apparently due to modification of the lower ionosphere resulting from extended X-ray emissions a few times higher than the background emission before the flare (Figures 2d and 2h), but much lower than the emission in the flare maximum.

## 4. Discussion

Our studies of lightning impulses in ELF frequencies were performed using two groups of WWLLN lightning data from African and American thunderstorm centers. The data from 2 days of 20 and 21 September, 2023, were analyzed, when a strong solar flare occurred in each day. In both examined data sets, the derived *v*/*c* parameter profile allows for determining the effective propagation speed of ELF impulses during the day and night. On the studied days, these velocities were between 0.96*c* and 0.85*c* for the night and the day for African lightning, respectively, and 0.92c and 0.82c for American lightning, with a scatter ~0.01c. In fact these extreme velocities can temporarily change due to ionospheric perturbations, for example, the solar terminator or the varying ionizing irradiation from the Sun, like X-ray flares presented here. The effective speed of lightning generated ELF electromagnetic impulses depends also on the propagation path between the source and the receiver relative to the varying ionosphere structure. One may note that the parameter *v*/*c* daily changes are clearly different between our lightning groups from Africa and America.

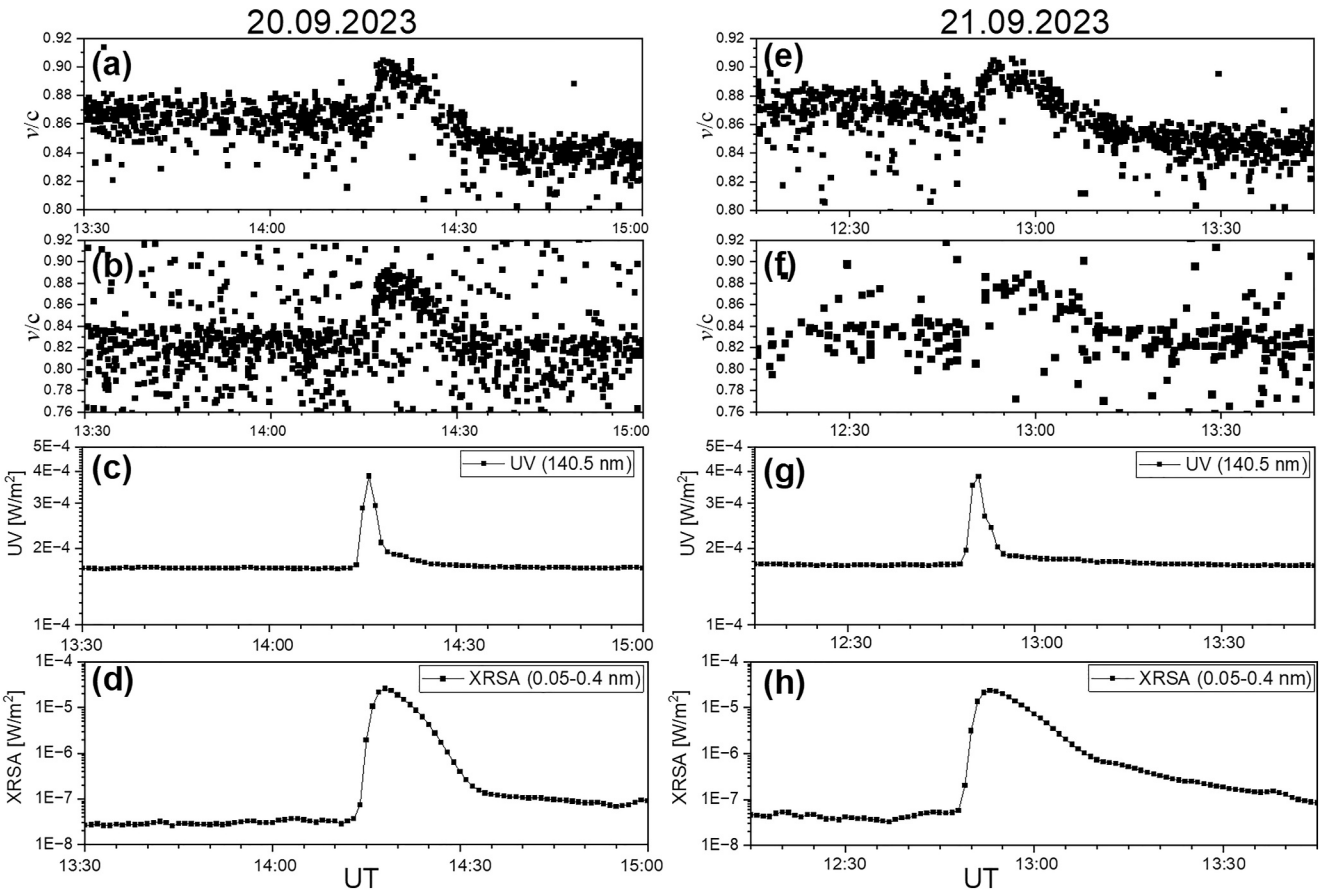


**Figure 4.** Distributions of the measured ELF propagation velocity *v/c* for WWLLN impulses (and accompanying UV and XRSA energy fluxes) in time ranges containing the solar flares: M8.2-class on 20 (left) September and M8.7-class on 21 (right) September 2023. For a 1.5 hr time periods, at the successive panels we present the parameter *v/c* for African events (panels a, e) and American events (panels b, f), while the GOES-16 ionized fluxes are given in UV (panels c, g) and X-ray in the range XRSA (panels d, h).

An increase in the signal propagation velocity was observed during two short periods (see Figure 4), coinciding with solar UV and X-ray ionizing radiation flashes recorded by the GOES-16 satellite. The time structures of the increase in the *v/c* profile are similar (only slightly delayed) to the XRSA profiles. However, in our observations we reveal also an interesting physical impact for ELF impulse propagation for increased XRSA emission, when strong irradiation during the solar flare allows for faster propagation, while lower irradiation after the flare (but still significantly higher than before it) leads to lower propagation speeds as compared to pre-flare conditions. Thus a possible wave guide transition occurs at intermediate X-ray intensities from higher ELF wave damping and lower propagation velocity, to low damping and high velocity at large fluxes. Figure 4 demonstrates a noticeable impact of the two M8-class flares that occurred during the analyzed period. In contrast, no effects associated with smaller C-class flares observed on these days are evident, indicating that this method, in its current form, does not provide sufficient sensitivity to detect C-class flares.

The change in ELF propagation velocity under the influence of a solar flare was first documented by Gołkowski et al. (2018). The signatures of the solar flares shown here are much more prominent and more closely matched to the XRSA flux. This is likely due to the recent improvements in timing accuracy of the Hylaty station, enabled by increased sampling frequency and more frequent oscillator correction with GPS timing as well as some differences in filtering algorithm. Overall, the observed variations in propagation velocity are in a good agreement with the Golkowski et al. (2018) theoretical model wherein the velocity increases in response to sharper electron density gradients in the ionospheric D-region. Observed variations in ELF propagation velocity, as described in this manuscript, offer valuable insights into the ionospheric D-region's electron density profile. Specifically, these variations can enhance the diagnosis of sharpness parameters ($\beta$) and reference heights ($h'$) within the two

parameter D-region model (Bannister, 1984; Golkowski et al., 2018). By providing empirical data on the sensitivity of ELF group velocity to electron density gradients, these observations help refine electron density profile predictions, particularly in distinguishing day-night transitions and assessing ionospheric perturbations. The approach is intended for improving the understanding and application of ELF remote sensing techniques in ionospheric studies.

For the African direction, the $\Delta A$ parameter profile around sunrise (~4:00 UT) and sunset (~17:00 UT) over the Hylaty station shows wavy perturbations associated with the terminator passing through the region where ELF signals from the African thunderstorm center are created. During these time ranges, such ELF impulses propagate in an ionosphere ionization gradient at the terminator, at small sliding angles or even parallel with respect the terminator. Consequently, these propagation conditions cause ELF wave refraction, and the azimuth determined from ELF measurements can significantly differ from the geographical azimuth.

Meanwhile, the $\Delta A$ profile for the American center where the ELF waves cross the terminator at large, nearly orthogonal angles does not exhibit such behavior. However, it should be noted that between 13:00 and 18:00, $\Delta A$ shows significant dispersion, while dispersions of fitted $\Delta t$ and $v/c$ are much less (if at all) modified. We hypothesize that $A_{\mathrm{ELF}}$ azimuths are perturbed by ionospheric inhomogeneities along the wave propagation paths at high geographic latitudes on the daytime Earth side, deviating in various directions from $A_g$ and leading to the large dispersion in the $\Delta A$ distribution. When inspecting Figure 1a one notes that paths of the impulses propagating from America to Hylaty are oriented latitudinal, perpendicular to the ionosphere changes between the equator and the poles. Thus such propagation across the involved ionization gradient is subject to refraction (Albini & Jahn, 1961; Denby et al., 1980; Decker et al., 1996, recently Ostrowski et al., 2024), which possibly explains the large systematic azimuth change of $-10°$ during the night, while for the impulses propagating from Africa along the ionospheric gradient we measure only $+1{,}5°$ azimuth deviation. We also note that the lower ionosphere is also known to be disturbed by high energy particles from auroral precipitation (Cummer et al., 1997), but this effect should be important at higher geographic latitudes.

The effect of thunderstorms on the D-region ionosphere electron density has been well documented using remote sensing in the VLF band (Golkowski et al., 2014; Haldoupis et al., 2004; Inan et al., 1993; Johnson et al., 1999) but not yet in the ELF band.

## 5. Conclusions

By utilizing an automated method that employs two different techniques for measuring thunderstorm activity (WWLLN and ELF), it is possible to determine the effective propagation speed of ELF impulses in the Earth-ionosphere waveguide and to identify deviations of $A_{\mathrm{ELF}}$ azimuths from the actual geographic azimuth values $A_g$. These results provide unique information about the state of the lower ionosphere and enable research on both long-term timescales (from days to years, influenced by solar activity) and short-term timescales (from minutes to hours, influenced by thunderstorms, energetic particle precipitation, ionospheric non-uniformities and solar flares).

The present paper shows our first illustrative study demonstrating abilities of the considered hybrid system applying WWLLN and ELF data to assess the impact of numerous solar weather conditions on the non-uniform state of the ionosphere. In our successive work the method is under development intended to elaborate it to become a standard tool for the analysis and monitoring of the lower layers of the ionosphere.

## Data Availability Statement

The ELF data used in the present analysis are available on-line from Kubisz and Mlynarczyk (2024). The data are still used in our successive studies, so we request that the provided data are only used for verification of our present and future publications. Using it for other studies requires our prior agreement.

**Acknowledgments**
Authors are grateful to Astronomical Observatory of the Jagiellonian University for continuous support of ELF research and operation of the WERA magnetic sensors' array. The development of ELA11 sensor has been supported by the National Science Centre, Poland, under Grant 2015/19/B/ST10/01055. The current research was funded by the National Science Centre, Poland, under Grant 2023/49/B/ST9/00142 (Z. Nieckarz) and Grant 2023/49/B/ST9/02777 (J. Kubisz and M. Ostrowski). Mark Golkowski was supported by National Science Foundation Awards AGS 2312282 and AGS 2320259 to University of Colorado Denver. János Lichtenberger was supported by TKP2021-NVA-29 project, provided by the Ministry of Culture and Innovation of Hungary from the National Research, Development and Innovation Fund.

## References

Albini, F. A., & Jahn, R. G. (1961). Reflection and transmission of electromagnetic waves at electron density gradients. *Journal of Applied Physics*, *32*(1), 75–82. https://doi.org/10.1063/1.1735964

Anderson, T. S., McCarthy, M. P., & Holzworth, R. H. (2020). Detection of VLF attenuation in the Earth-ionosphere waveguide caused by X-class solar flares using a global lightning location network. *Space Weather*, *18*(3), e2019SW002408. https://doi.org/10.1029/2019SW002408

Bannister, P. (1984). ELF propagation update. *IEEE Journal of Oceanic Engineering*, *9*(3), 179–188. https://doi.org/10.1109/10.1109/JOE.1984.1145609

Barr, R., Jones, D. L., & Rodger, C. J. (2000). ELF and VLF radio waves. *Journal of Atmospheric and Solar-Terrestrial Physics*, *62*(17–18), 1689–1718. https://doi.org/10.1016/S1364-6826(00)00121-8

Burch, H. C., & Moore, R. C. (2024). Polarization-based VLF remote sensing of transient ionospheric disturbances. *IEEE Transactions on Geoscience and Remote Sensing*, *62*, 2006509. https://doi.org/10.1109/TGRS.2024.3469381

Burkholder, B. S., Hutchins, M. L., McCarthy, M. P., Pfaff, M. P., & Holzworth, R. H. (2013). Attenuation of lightning-produced sferics in the Earth-ionosphere waveguide and low-latitude ionosphere. *Journal of Geophysical Research*, *118*(6), 3692–3699. https://doi.org/10.1002/jgra.50351

Cummer, S. A., Bell, T. F., Inan, U. S., & Chenette, D. L. (1997). VLF remote sensing of high energy auroral particle precipitation. *Journal of Geophysical Research*, *102*(A4), 7477–7484. https://doi.org/10.1029/96JA03721

Decker, C. D., Eder, D. C., & London, R. A. (1996). Ionization-induced refraction in recombination X-ray lasers. *Physics of Plasmas*, *3*(1), 414–419. https://doi.org/10.1063/1.871868

Denby, M., Bullough, K., Alexander, P., & Rycroft, M. (1980). Observational and theoretical studies of a cross meridian refraction of VLF waves in the ionosphere and magnetosphere. *Journal of Atmospheric and Terrestrial Physics*, *42*(1), 51–60. https://doi.org/10.1016/0021-9169(80)90123-3

Gołkowski, M., Gross, N. C., Moore, R. C., Cotts, B. R. T., & Mitchell, M. (2014). Observation of local and conjugate ionospheric perturbations from individual oceanic lightning flashes. *Geophysical Research Letters*, *41*(2), 273–279. https://doi.org/10.1002/2013GL058861

Golkowski, M., Renick, C., & Cohen, M. B. (2021). Quantification of ionospheric perturbations from lightning using overlapping paths of VLF signal propagation. *Journal of Geophysical Research: Space Physics*, *126*(5), e2020JA028540. https://doi.org/10.1029/2020JA028540

Golkowski, M., Sarker, S. R., Renick, C., Moore, R. C., Cohen, M. B., Kulak, A., et al. (2018). Ionospheric D region remote sensing using ELF sferic group velocity. *Geophysical Research Letters*, *45*(23), 12739–12748. https://doi.org/10.1029/2018GL080108

Gross, N. C., & Cohen, M. B. (2020). VLF remote sensing of the D region ionosphere using neural networks. *Journal of Geophysical Research: Space Physics*, *125*(1), e2019JA027135. https://doi.org/10.1029/2019JA027135

Haldoupis, C., Neubert, T., Inan, U. S., Mika, A., Allin, T. H., & Marshall, R. A. (2004). Subionospheric early VLF signal perturbations observed in one-to-one association with sprites. *Journal of Geophysical Research*, *109*(A10303). https://doi.org/10.1029/2004JA010,651

Inan, U. S., Rodriguez, J. V., & Idone, V. P. (1993). VLF signatures of lightning-induced heating and ionization of the nighttime D-region. *Geophysical Research Letters*, *20*(21), 2355–2358. https://doi.org/10.1029/93GL02620

Johnson, M. P., Inan, U. S., Lev-Tov, S. J., & Bell, T. F. (1999). Scattering pattern of lightninginduced ionospheric disturbances associated with early/fast VLF events. *Geophysical Research Letters*, *26*(15), 2363–2366. https://doi.org/10.1029/1999GL900521

Kubisz, J., Gołkowski, M., Mlynarczyk, J., Ostrowski, M., & Michalec, A. (2024). New method for determining azimuths of ELF signals associated with the global thunderstorm activity and the Hunga Tonga volcano eruption. *Journal of Geophysical Research: Atmospheres*, *129*(4), e2023JD040318. https://doi.org/10.1029/2023JD040318

Kubisz, J., & Mlynarczyk, J. (2024). A set of measurement data from the ELA11 magnetometer from September, 2023 [Dataset]. *Hylaty Station, Poland*. https://doi.org/10.57903/UJ/LOGPP8

Kulak, A., Kubisz, J., Klucjasz, S., Michalec, A., Mlynarczyk, J., Nieckarz, Z., et al. (2014). Extremely low frequency electromagnetic field measurements at the Hylaty station and methodology of signal analysis. *Radio Science*, *49*(6), 361–370. https://doi.org/10.1002/2014RS005400

Liu, J., Huang, J., Li, Z., Zhao, Z., Zeren, Z., Shen, X., & Wang, Q. (2023). Recent advances and challenges in Schumann resonance observations and research. *Remote Sensing*, *15*(14), 3557. https://doi.org/10.3390/rs1514355

Nickolaenko, A. P., & Hayakawa, M. (2002). *Resonances in the earth-ionosphere cavity*. Kluwer Academic Publisher. 380.

Nieckarz, Z. (2016). Imprints of natural phenomena and human activity observed during 10 Years of ELF magnetic measurements at the hylaty geophysical station in Poland. *Acta Geophysica*, *64*(6), 2591–2608. https://doi.org/10.1515/acgeo-2016-01

Nieckarz, Z., Kulak, A., Zieba, S., & Odzimek, A. (2011). Cloud-to-ground lightning dipole moment from simultaneous observations by ELF receiver and combined direction finding and time-of-arrival lightning detection system. *Journal of Geophysical Research*, *116*(D8), D08107. https://doi.org/10.1029/2010JD014736

Ostrowski, M., Gołkowski, M., Kubisz, J., Michalec, A., Mlynarczyk, J., & Nieckarz, Z. (2024). Refraction of ELF electromagnetic waves by the ionospheric gradients at the day/night terminator measured at the Hylaty station. *Journal of Geophysical Research: Space Physics*, *129*(12), e2024JA033274. https://doi.org/10.1029/2024JA0332

Richardson, D. K., & Cohen, M. B. (2023). Unifying VLF transmitter and sferic modeling efforts via tomography. *Journal of Geophysical Research: Space Physics*, *128*(11), e2023JA031989. https://doi.org/10.1029/2023JA031989

Rodger, C. J., Brundell, J. B., Dowden, R. L., & Thomson, N. R. (2004). Location accuracy of long distance VLF lightning location network. *Annals of Geophysics*, *22*(3), 747–758. https://doi.org/10.5194/angeo-22-747-2004

Said, R. K., & Murphy, M. J. (2016). GLD 360 upgrade: Performance analysis and applications. https://api.semanticscholar.org/CorpusID:53645357